Survey on Amacrine Cells Coupling to Retrograde-Identified Ganglion Cells in the Mouse Retina

Ji-Jie Pang,[1] David L. Paul,[2] and Samuel M. Wu[1]

[1]Department of Ophthalmology, Baylor College of Medicine, Houston, Texas
[2]Department of Neurobiology, Harvard Medical School, Boston, Massachusetts

Correspondence: Ji-Jie Pang, Department of Ophthalmology, Baylor College of Medicine, One Baylor Plaza, NC-205, Houston, TX 77030; jpang@bcm.edu.

Submitted: January 29, 2013
Accepted: June 22, 2013

Citation: Pang J-J, Paul DL, Wu SM. Survey on amacrine cells coupling to retrograde-identified ganglion cells in the mouse retina. *Invest Ophthalmol Vis Sci*. 2013;54:5151–5162. DOI:10.1167/iovs.13-11774

Purpose. Retinal amacrine cells (ACs) may make inhibitory chemical synapses and potentially excitatory gap junctions on ganglion cells (GCs). The total number and subtypes of ACs coupled to the entire GC population were investigated in wild-type and three lines of transgenic mice.

Methods. GCs and GC-coupled ACs were identified by the previously established LY-NB (Lucifer yellow–Neurobiotin) retrograde double-labeling technique, in conjunction with specific antibodies and confocal microscopy.

Results. GC-coupled ACs (NB-positive and LY-negative) comprised nearly 11% of displaced ACs and 4% of conventional ACs in wild-type mice, and were 9% and 4% of displaced ACs in *Cx45*$^{-/-}$ and *Cx36/45*$^{-/-}$ mice, respectively. Their somas were small in *Cx36/45*$^{-/-}$ mice, but variable in other strains. They were mostly γ-aminobutyric acid (GABA)-immunoreactive (IR) and located in the GC layer. They comprised only a small portion in the AC subpopulations, including GABA-IR, glycine-IR, calretinin-IR, 5-HT-accumulating, and ON-type choline acetyltransferase (ChAT) ACs in wild-type and ChAT transgenic mice (ChAT-tdTomato). In the distal 80% of the inner plexiform layer (IPL), dense GC dendrites coexisted with rich glycine-IR and GABA-IR. In the inner 20% of the IPL, sparse GC dendrites presented with a major GABA band and sparse glycine-IR.

Conclusions. Various subtypes of ACs may couple to GCs. ACs of the same immunoreactivity may either couple or not couple to GCs. Cx36 and Cx45 dominate GC-AC coupling except for small ACs. The overall potency of GC-AC coupling is moderate, especially in the proximal 20% of the IPL, where inhibitory chemical signals are dominated by GABA ACs.

Keywords: retrograde labeling, connexin, GABA, NOS, 5-HT, ChAT

Visual signals generated in the retina are passed onto the brain via the optic nerve, which is comprised of axons of retinal ganglion cells (GCs). As one of the most important neuronal populations in the retina, GCs receive primarily chemical inputs from presynaptic neurons. Most chemical inputs from bipolar cells (BCs) are excitatory for GCs and those from amacrine cells (ACs), whether γ-aminobutyric acid (GABA)-ergic or glycinergic, are usually inhibitory. However, as "inhibitory neurons," ACs may also form electrical synapses with GCs.[1,2] ACs in the vertebrate retina mostly generate depolarizing light responses[3–7] at either or both light onset and offset upon illumination of the center of the receptive field, thus these sign-preserving gap-junctions from ACs are potentially excitatory for their coupled GCs. Therefore, ACs may modify GC outputs in two different ways, yet it is unknown how many ACs are coupled with GCs,[8] and the overall strength of GC-AC coupling in the entire retina has not been evaluated.

In the mammalian retina, gap junctions have been found to be permeable to glycine, which was first revealed in the junctions between cone depolarizing bipolar cells (DBC_Cs) and AII ACs.[9,10] Gap junctions between GCs and ACs are permeable to Neurobiotin (NB) and likely permeable to GABA, as well.[8,11] GCs and ACs in the mammalian retina are both classified into more than 20 morphological subtypes.[6,8,12–14] NB filling of individual GCs, facilitated by electric currents, has contributed much to the study of GC-AC coupling. However, for most GC subtypes, the identity and number of coupled ACs are unclear.[8] GCs and ACs may both reside in the GC layer (GCL) and inner nuclear layer (INL), and they are not obviously distinguishable by soma size,[15,16] axons,[17,18] or dendritic tree shape.[6,15,19] Amacrine cells are often identified immunologically by antibodies against GABA, glycine,[20,21] Choline acetyltransferase (ChAT),[20,22] tyrosine hydroxylase (TH),[23–25] and neuronal or brain-type nitric oxide synthase (nNOS or bNOS),[26–28] while antibodies against calcium-binding proteins, such as parvalbumin (PV)[29–31] and calretinin (CR),[32–34] may label GCs. A more reliable way to distinguish GCs from ACs, however, is retrograde labeling of GCs.[35–37] In the retrogradely labeled mouse retina, the specificity of GABA, glycine, ChAT, and nNOS antibodies in labeling retinal ACs has been recently confirmed,[28] but similar investigations have not been done for TH,[38] CR,[32–34] and PV.[29–31]

Of the multiple subtypes of ACs, GABA ACs are the only subtype that have been confirmed to couple with GCs.[39,40] It is still unknown how many GABA ACs and other subtypes of ACs are coupled with GCs and whether all the cells in an individual immunological subpopulation contact the same number and types of GCs or ACs. Cx36 and Cx45 are important gap junctional proteins for GC-AC coupling,[2,41,42] but it is still unclear whether they are critical for all GC-AC coupling.

NB is widely used to study gap junctions in the central nervous system[1,9,10,28] and Lucifer yellow (LY) is a fluorescent dye that is commonly used to reveal individual cell morphology.[21,43,44] Neuronal gap junctions are known to be impermeable to LY.[45] Using these two dyes, we have previously established a retrograde labeling method for identification of the entire retinal GC population and simultaneous visualization of all the coupling partners.[11,28] The labeling specificity and efficiency on the whole GC population have been examined and confirmed. The two dyes are actively transported into GC somas by GC axonal transportation and NB is freely passed into coupled ACs via gap junctions. This method provides a novel approach for revealing GC-coupled ACs in the whole mouse retina. In this paper, by using this technique, we studied the GC-AC coupling, focusing on: the function of Cx36 and Cx45 in the overall GC-AC coupling; the total population of coupled ACs; the variety of coupled ACs; and the coupling frequency of AC subtypes.

Methods

Animals

The animals used in this study were C57BL/6J, B6.Cg-Gt(ROSA)26Sor$^{tm14(CAG-tdTomato)Hze}$/J (stock# 007914) and B6;129S6-Chat$^{tm1(cre)Lowl}$/J (stock# 006410) mice from Jackson Laboratory (Bar Harbor, ME). Retinal ChAT cells may be revealed by expression of the red fluorescent protein variant, tdTomato, following Cre-mediated recombination. Generation of the *Cx45*$^{-/-}$ and *Cx36/45*$^{-/-}$ mice was described in previous publications,[46,47] in which neuronal specific Cx45 was conditionally knocked out. The mice were 2- to 8-month-old males and females. All procedures used in this study followed the NIH animal care guidelines and ARVO Statement for the Use of Animals in Ophthalmic and Vision Research, as well as the relevant requirements of the Baylor College of Medicine Animal Care and Use Committee. All mice were dark-adapted for 1 to 2 hours prior to the experiment. Animals were anesthetized with an intraperitoneal injection of ketamine (200 mg/kg) and xylazine (10 mg/kg). The eyes were enucleated after the animals were deeply anesthetized. Animals were killed by overdose of the anesthesia thereafter.

Antibodies and Specificity

The primary antibodies that were used in this study have been used in previous reports, including polyclonal guinea pig anti-GABA (1:1K, AB175; Chemicon, Temecula, CA)[48]; polyclonal goat anti-ChAT (1:100, AB144P; Chemicon)[22]; polyclonal rabbit anti-TH (1:500, AB152; Chemicon)[20,22]; rat anti-glycine antiserum (1:1000; a gift from David Pow, University of Queensland, Brisbane, Australia)[20,49,50]; rabbit anti-PKCα antiserum (1:1000, P4334; Sigma-Aldrich, Milwaukee, WI)[28,51] and rabbit anti-nNOS antiserum (1:4000, N7155, also abbreviated as anti-bNOS; Sigma-Aldrich).[28,52] To label 5-HT-accumulating cells, retinas were incubated in 2 μM 5-HT containing medium for 15 minutes before fixation. Rabbit anti-5-HT antiserum was obtained from Immunostar, Inc. (1:500, Hudson, WI).[11] The specificity of these primary antibodies has been demonstrated in the previous studies and their staining patterns in our results were similar to the previous reports.

Retrograde Labeling of GCs and Immunocytological Staining

Previously established techniques were precisely followed.[11] Animals were dark-adapted and eyeballs were enucleated under the illumination of dim red light. A mixture of Neurobiotin, a gap-junction-permeable dye (NB, MW 322.85; Vector Laboratories, Burlingame, CA), and Lucifer yellow, a less permeable dye (LY, MW 457.24; Sigma-Aldrich, St. Louis, MO),[9,45,53] was used for the labeling. Freshly dissected eyeballs with an attached optic nerve stump were chosen for retrograde labeling. First, the nerve stump was dipped into a small drop (3 μL) of a cocktail that contained 3% LY and 8% NB in the internal solution[28] for 20 minutes. Afterward, the eyeball was thoroughly rinsed with oxygenated Ames medium (Sigma-Aldrich) to remove the extra dye. Then, the eyeball was dissected under infrared illumination. The dark-adapted eyecup with intact retina and sclera tissue was transferred into fresh oxygenated Ames medium (Sigma-Aldrich) and kept at room temperature for 40 minutes under a 10-minute dark, 10-minute light cycle. Under this adaptation-neutral condition, ON and OFF retinal neurons can both be activated and adaptation-dependent bias on the survey of GC-coupled ACs[54–56] may be minimized. The Ames medium (Sigma-Aldrich) in which retinas were incubated was replaced every few minutes by fresh medium during the labeling. Following the light cycle, the whole retina was isolated from the sclera and fixed in darkness for 30 to 45 minutes at room temperature. The fixed retinas were blocked with 10% donkey serum (Jackson ImmunoResearch, West Grove, PA) in TBS (D-PBS) with 0.5% Triton X-100 (Sigma-Aldrich) and 0.1% NaN_3 (Sigma-Aldrich) for 2 hours at room temperature or at 4°C overnight to reduce nonspecific labeling.

All retinas were dissected under the same experiment conditions. A vibratome (Pelco 102, 1000 Plus; Ted Pella, Inc., Redding, CA) was used to prepare retinal slices. Whole retinas were imbedded in low gel-point agarose (Sigma-Aldrich) and trimmed into a $10 \times 10 \times 10$ mm^3 block. The block was glued onto a specimen chamber mounted on the vibratome and subsequently cut into 40-μm thick vertical sections in PBS solution. Whole retinas and free-floating sections were incubated in primary antibodies in the presence of 3% donkey serum-TBS for 3 to 5 days in 4°C. Controls were also processed without primary antibodies. Following several rinses, the slices and whole retinas were then transferred into Cy3-, Cy5-, or Alexa Fluor 488-conjugated streptavidin (1:200, Jackson ImmunoResearch), with Cy3- and/or Cy5-conjugated secondary antibodies (1:200, Jackson ImmunoResearch) and/or Alexa Fluor 488-conjugated secondary antibodies (1:200; Molecular Probes, Eugene, OR), in 3% normal donkey serum-TBS solution at 4°C overnight. A nuclear dye, TO-PRO-3 (0.5 μL/mL, Molecular Probes) was used with the secondary antibody to visualize nuclei in retinas.[11] After extensive rinsing, the retinal preparations were cover-slipped. Two small pieces of filter paper (180-μm thick, MF-membrane filters; Millipore, Billerica, MA) were mounted beside whole retinas to prevent them from being over-flattened. Consistent labeling was obtained from both slice preparations and whole retinas, in line with previous reports.[11,57]

Identification of GCs, GC-Coupled ACs, and Displaced ACs

We have previously shown that the double retrograde labeling technique was reliable and specific for visualization of the entire retinal GC population.[11,28] The somas in the GCL, inner plexiform layer (IPL), and INL that contained LY were identified as GCs. All GC somas, thereby identified, contained NB and thus all GC somas were positive for both LY and NB. But NB labeled more somas than LY did. These NB-labeled, LY-negative somas, often weakly NB positive, were not glial cells.[11] They were identified as GC-coupled neurons. These cells were further examined with AC markers to confirm their

Investigative Ophthalmology & Visual Science

AC identity in this study (see results). The GC-coupled ACs were separately counted in the GCL and INL, together with GCs and displaced ACs (see below). Both whole-mount retinas and vertical retinal slices were used for the study.

TO-PRO-3 labeled all nuclei in the retina. The total TO-PRO-3 labeled nuclei in the GCL, excluding those from non-neurons,[11] were counted as total neurons there. Total displaced ACs were calculated by deducting the total GC number from the total neuron number in the GCL. Total displaced ACs in wild-type mice revealed previously under the same experimental conditions comprise 56% of the total neurons in the GCL.[11]

The retinal preparations were observed with a laser scanning confocal microscope (LSM 510; Carl Zeiss Meditec, Jena, Germany). LSM software was used to take images. The background labeling, identified by diffuse and ambiguous signals presented between brightly labeled profiles, was set as zero value or baseline; the brightest signals were set as the maximum or saturating point. This setting controlled the range of signals that were taken into micrographs. All conclusions in our results were based on original confocal images. Images were further processed using a graphics editing program (Adobe Photoshop v. 9.0.2; Adobe Systems, San Jose, CA) for presentation purposes. For better visibility, some images were presented in black and white, with fluorescent signals in black against a bright background (Figs. 2, 4, insets; Fig. 3, right panels). For the same reason, some color images (Fig. 3, left panels; Fig. 5) were also inverted, in which fluorescent signals were presented against a bright background.

Results

The proximal margin of the IPL (against the GCL) was defined as 100% of the IPL depth, and this definition was used to describe the location of neuronal processes in the IPL. In retrogradely labeled whole retinas, NB and LY highlighted axon bundles, axon-bearing somas, and neuronal processes in the GCL and INL throughout the entire retina. The fluorescent signals presented a diffusion gradient with the strongest in axons, medium in the somas, and relatively weak in the dendritic arbors. The gradient made it hard to show all the cellular structures clearly with a single exposure time. In most of the micrographs, we intended to show GC somas, thus GC axons may appear to be overexposed and some dendritic arbors may be too weak to visualize.

To determine the percentage of displaced ACs coupled to GCs, we primarily used flat-mount retina preparations. Briefly, in each retina we took the same number of confocal images of the GCL from the central and peripheral retina, and in every image, we counted LY-positive GC somas, NB-positive somas, and TO-PRO-3 labeled nuclei. The difference between the counts of LY-positive and NB-positive somas was the number of displaced ACs coupled with GCs. The difference between the counts of TO-PRO-3 labeled neuronal nuclei and LY-positive somas yielded the total number of displaced ACs. Therefore, the percentage of displaced ACs coupled to GCs is derived from the LY-negative/NB positive somas in the GCL as a fraction of the total displaced ACs.

To determine the percentage of coupled ACs in subpopulations of ACs, we primarily used retinal slices. For ChAT-ACs, we used both slice and flat-mount preparations. We took multiple images from different locations in retinal slice preparations and randomly chose images for cell counting. ACs were identified by their immunoreactivity (IR) to an AC marker and the lack of LY. ACs in the GCL and those in the INL were separately examined. For each selected image, the total number of ACs and the number of NB-positive ACs were counted. Most ACs are either GABA ACs or glycine ACs, with each making up nearly half of the total AC population.[21,58–62] Therefore, the percentage of all ACs in the INL that are coupled to GCs can be calculated as the average of the percentage of GABA ACs and the percentage of glycine ACs coupled to GCs.

Total Number of GC-Coupled ACs in Wild-Type and Knockout Mice

GC-coupled neurons were observed in both the GCL and INL. We estimated that the number of GC-coupled neurons, assumed to be ACs, in the GCL was equal to 11% of the total displaced ACs and 13% of the number of GCs ($n = 1150$) in the wild-type mouse. GC-coupled ACs in the GCL as a percentage of displaced ACs was reduced to 9% ($n = 1356$) in the *Cx45*$^{-/-}$ mouse and to 4% in the *Cx36/Cx45*$^{-/-}$ mouse ($n = 1365$) (Fig. 1). Coupled ACs in the wild-type mice had variable soma sizes, ranging from large (~15 μm) to very small (~5 μm). Coupled cells with preserved NB labeling showed both medium (~10 μm) and small soma size in *Cx45*$^{-/-}$ mice and small soma size in *Cx36/Cx45*$^{-/-}$ mice (Fig. 1). The data demonstrate that Cx36 and Cx45 play significant roles in GC-AC coupling, except for small ACs.

To classify GC-coupled ACs, we chose eight antibodies, including antibodies against GABA, glycine, ChAT, TH, nNOS, 5-HT, CR, and PV, to stain the retina. In the retrogradely labeled mouse retina, the specificity of GABA, glycine, ChAT, and nNOS antibodies in labeling retinal ACs has been recently confirmed,[28] but similar investigations have not been done for TH, CR, and PV. The ChAT ACs were studied in both wild-type and ChAT-transgenic mice.

Specificity of GABA, Glycine, ChAT, nNOS, and TH Antibodies for Identification of ACs in the GCL and INL

GABA and glycine are classic AC markers. ChAT, nNOS, and TH are colocalized with GABA, and they have been used for identification of ACs as well. Consistent with a previous report,[11] we did not observe glycine-, ChAT-, TH- or nNOS-IR in retrogradely identified GCs in the GCL or INL. GC somas were occasionally weakly GABA-IR, but they were easily distinguished from ACs due to their high LY content. The data prove the specificity of GABA, glycine, ChAT, TH, and nNOS antibodies for identification of ACs.

With somas of GCs and ACs being clearly labeled to serve as the boundaries of the IPL, we reexamined staining patterns of the antibodies in the IPL (Figs. 2, 3). GABA-IR in the IPL appeared as multiple bands. Five GABA-IR bands were revealed around 0%, 30% to 40%, 50%, 60%, and 70% to ~100% of the IPL depth. The major GABA band at 70% to ~100% of the IPL depth comprised nearly 40% of the total thickness of GABA-IR bands. The thinner GABA bands were found at the locations of the TH band (0% of the IPL depth); two 5-HT bands (0% and 40% of the IPL); the central nNOS band (50% of the IPL depth); and ChAT bands (30% and 60% of the IPL depth). Glycine-IR processes ramified diffusely in the IPL. Nearly one-third of GABA-IR or glycine-IR somas were strongly stained; two-thirds were weakly labeled. ChAT-IR somas ($n = 136$) were found in the INL (48%) and GCL (52%). The location of ChAT-bands and the distribution of ChAT-somas were similar in the wild-type and ChAT transgenic mice. TH-IR showed a single dense but narrow band along the distal margin of the IPL. TH-IR somas were mostly found in the INL. On a few occasions, TH-IR somas were seen in the GCL, and they appeared to be smaller

Investigative Ophthalmology & Visual Science

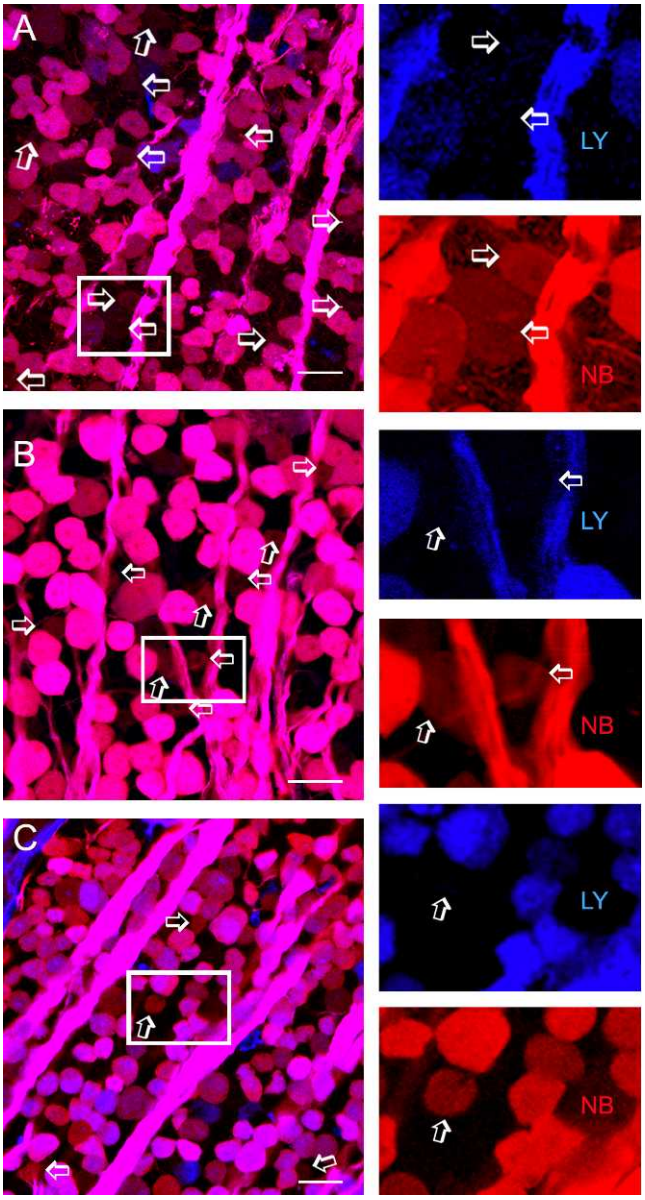

FIGURE 1. ACs coupled to GC populations. Confocal micrographs from flat-mounted retinas from the wild-type mouse (**A**), conditional neuron-specific *Cx45*$^{-/-}$ mouse (**B**), and *Cx36/Cx45*$^{-/-}$ mouse (**C**) that were retrogradely double-labeled for LY (*blue*), and NB (*red*). A small population of displaced ACs (*arrows* and *insets*) is weakly positive for NB but negative for LY. The *blue* and *red* channels of each *inset* are separately depicted to the right. Coupled ACs show large to small soma size in wild-type mice, medium to small somas in *Cx45*$^{-/-}$ mice but mostly small somas in *Cx36/45*$^{-/-}$ mice. The number of coupled ACs is reduced more severely in *Cx36/45*$^{-/-}$ than in *Cx45*$^{-/-}$ mice. GCL, GC layer. *Scale bar*: 20 μm.

than normally localized somas (Fig. 2). Strongly labeled type-I nitrergic (NI) AC somas[28] in the INL sent dendrites to the center of the IPL. Labeling patterns of GABA, glycine, ChAT, nNOS, and TH in our results were similar to previous findings (Fig. 2).

In addition, we compared the location of the processes of ACs and retrogradely identified GCs in the IPL (Fig. 3). The results revealed a high and nearly even density of LY-positive GC dendrites in the distal 80% of the IPL, where GABA bands, ChAT bands, 5-HT-bands (see following section), and dense glycine-IR were located. In the inner 20% of the IPL, however, GC dendrites and glycine-IR were sparse, coexisting with the major GABA band and PKCα-IR globules.

We observed that some somas of GABA-, glycine-, ChAT- or nNOS-IR-ACs were weakly positive for NB, but negative for LY (Fig. 2). The distribution of NB signals in the IPL was similar to that of the LY signal. NB signals in the somas of GC-coupled ACs were usually a few to 10 times weaker than that of GCs (Figs. 2, 3). In some instances, dendrites of GC-coupled ACs possessed brighter NB signals than their somas (Fig. 2), indicating that coupled ACs obtained NB from dendrites where they were coupled to GCs. In overexposed confocal micrographs (Figs. 2B, 2D), NB and GABA-IR were colocalized throughout the distal 80% of the IPL, and the colocalization of NB and glycine-IR was concentrated around 15 to ~80% of the IPL depth. This indicates that GC-AC coupling mostly occurs in the distal 80% of the IPL.

Specificity of 5-HT, CR, and PV Antibodies for Identification of ACs or GCs

We examined the specificity of 5-HT (Fig. 4), PV, and CR (Fig. 5) for labeling ACs and GCs in retrogradely labeled retinas. We have previously reported 5-HT-accumulating GCs in the mouse retina.[11] Here we further observed that nearly one-third of 5-HT-accumulating somas in the inner retina were not labeled by LY and were thus identified as 5-HT ACs; the rest were positive for LY and classified as GCs. 5-HTACs were often found in the INL. The cells sent dendritic processes to 0% and 40% of the IPL depth, where two weak 5-HT bands were formed. A few dendrites were also observed to ascend into the OPL. 5-HT-IR was generally more intensive in GCs than in ACs, but a small portion of 5-HT ACs was brightly 5-HT-IR. Therefore, accumulation of 5-HT is not a safe criterion to distinguish GCs from ACs.

In the inner retina, PV-IR somas were primarily found in the GCL, and CR-IR somas were present in both the GCL and INL. In the IPL, CR-IR revealed three bands near 30%, 50%, and 60% of the IPL depth, close to the central nNOS-band (at 50% of the IPL depth) and two ChAT bands. In the GCL, PV-IR somas were mostly GCs (77%, 20/26). CR-IR somas in the GCL, however, were mainly displaced ACs (71%, 74/104). Most retrogradely identified GCs that we observed were negative for PV (82%, 107/127) or negative for CR (74%, 97/127), thus PV-IR GCs and CR-IR GCs each accounted for nearly one-fifth of the GC population. Very weak PV-IR was colocalized with bright CR-IR in a few GCs and CR-IR displaced ACs. PV-IR GCs had large somas, while CR-IR GCs usually possessed small- to medium-sized somas. CR-IR was also present in axons in both flat-mounted retinas and retinal slices. In some retinal vertical sections, CR-IR axons appeared as clusters of dots, whose shape depended on the section angle and axonal directions (Fig. 5). In flat-mount retinas, somas negative for retrograde dyes could overlap with CR-IR axons, and these were not identified as GCs in this report. In the GCL, PV-IR, and CR-IR ACs comprised about 3.7% (6/155) and 47.7% (74/155) of the total displaced ACs, respectively. Some CR-IR ACs contained weak NB signal and were identified as GC-coupled ACs.

These results demonstrate that GCs and ACs in the GCL and INL were not distinguishable by 5-HT-IR, PV-IR, or CR-IR.

Subpopulations of GC-Coupled ACs

GC-coupled neurons in wild-type mice were individually identified as ACs by localization in the GCL or INL, absence of LY, presence of NB, and immunoreactivity for glycine, GABA,

Investigative Ophthalmology & Visual Science

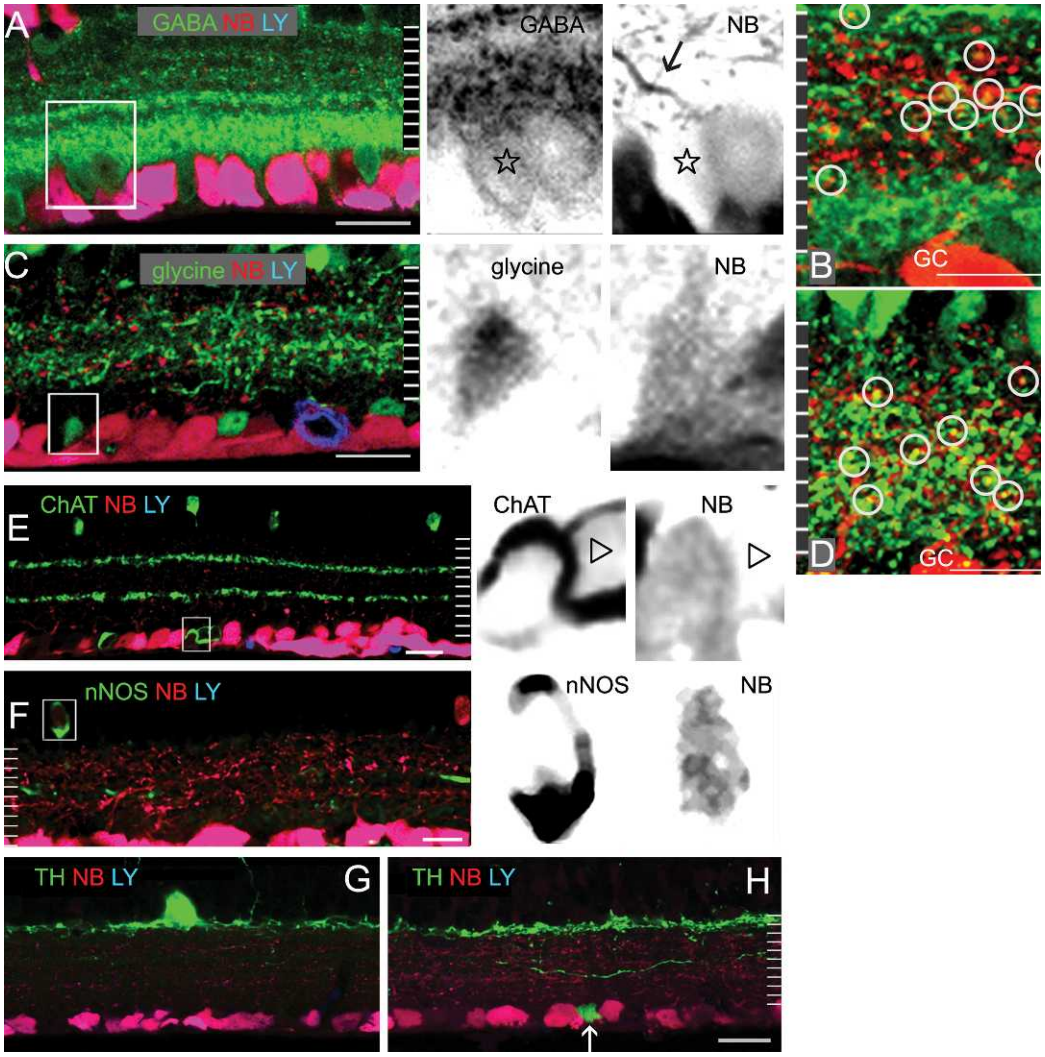

Figure 2. Identification of GCs and GC-coupled ACs. Single confocal micrographs of retinal vertical sections that were retrograde-labeled by LY (*blue*) and NB (*red*), and further stained for GABA (**A**, **B**); glycine ([**C**, **D**], *green*); ChAT (**E**); nNOS (**F**); or TH (**G**, **H**) in *green*. LY-labeled GCs are negative for glycine, ChAT, nNOS, and TH-IR. The *red* and *green* channels of *insets* from (**A**, **C**, **E**, **F**) are separately depicted in *black*, showing GC-coupled ACs that are negative for LY and positive for NB and an AC marker, as well as solitary ACs that are negative for LY and NB but positive for GABA (*star*, [**A**]) or ChAT (*triangle*, [**E**]). A brightly NB-labeled dendrite (*arrow*, [**A**]) is visible from a GABA-IR GC-coupled AC. GABA-IR, ChAT-IR, and glycine-IR AC somas are visible in the GCL and INL. A relatively shorter exposure time is used for identification of ChAT cells. At 70% to ~100% of IPL depth, a major GABA-IR band appears to be broad and intense where glycine-IR is sparse. In overexposed micrographs of the IPL (**B**, **D**), the colocalization (*circles*, [**B**]) of NB with GABA-IR is commonly seen at 0% to 80% of the IPL depth; and the colocalization of NB with glycine-IR (*circles*, [**D**]) is concentrated at approximately 15% to 80% of the IPL depth. Two ChAT-IR bands are present at approximately 30% and 60% of the IPL depth. TH-IR forms a dense band near the distal margin of the IPL. Some dendrites ascend to the OPL and some descend to the IPL. A small TH-IR soma is present in the GCL (*arrow*, [**H**]). *Scale bar*: 20 μm.

ChAT, nNOS, or TH. Since GCs and ACs could both be CR-, PV-, or 5-HT-IR, such labeled cells relied on retrograde labeling to be identified as ACs or GCs in this report. To distinguish a signal from background noise and compare the intensity of signals in an image, we also measured signal brightness using graphics editing software (Adobe Systems). Upon detecting the cursor location in the image, the program showed the brightness of a pixel there for every color channel with a number in the range of 0 to 255. NB signals in the coupled cells was usually more than 2 times brighter than the background staining in the adjacent area. Using these criteria, we identified more than five subtypes of GC-coupled ACs (i.e., GABA-IR, nNOS-IR, glycine-IR, CR-IR, ChAT, and 5-HT accumulating ACs).

In the first section, without using AC markers, we observed that nearly 11% of the total displaced ACs were coupled with GCs. Here, with GABA and glycine antibodies, we observed that GABA-IR and glycine-IR coupled ACs comprised nearly 10.2% (11/118) and 1.7% (3/176), respectively, of the total displaced ACs, consistent with the results in the first section, and that these GC-coupled ACs in the GCL were mostly GABA-IR (80%). In the INL, further observations (Table) revealed that around 4% of GABA and glycine ACs were involved in the coupling. Additionally, 9% of the displaced 5-HT-IR ACs were GC-coupled ACs, while in the INL 6% of nNOS ACs and 10% of 5-HT accumulating ACs were coupled with GCs. Coupled nNOS ACs ramifying in the center of the IPL were previously identified as NI ACs.[11]

In wild-type mice, ChAT-IR ACs in the INL were not found to be coupled with GCs, but 2% of the ChAT-IR ACs in the GCL were labeled by NB (Table). To verify this result, we

Investigative Ophthalmology & Visual Science

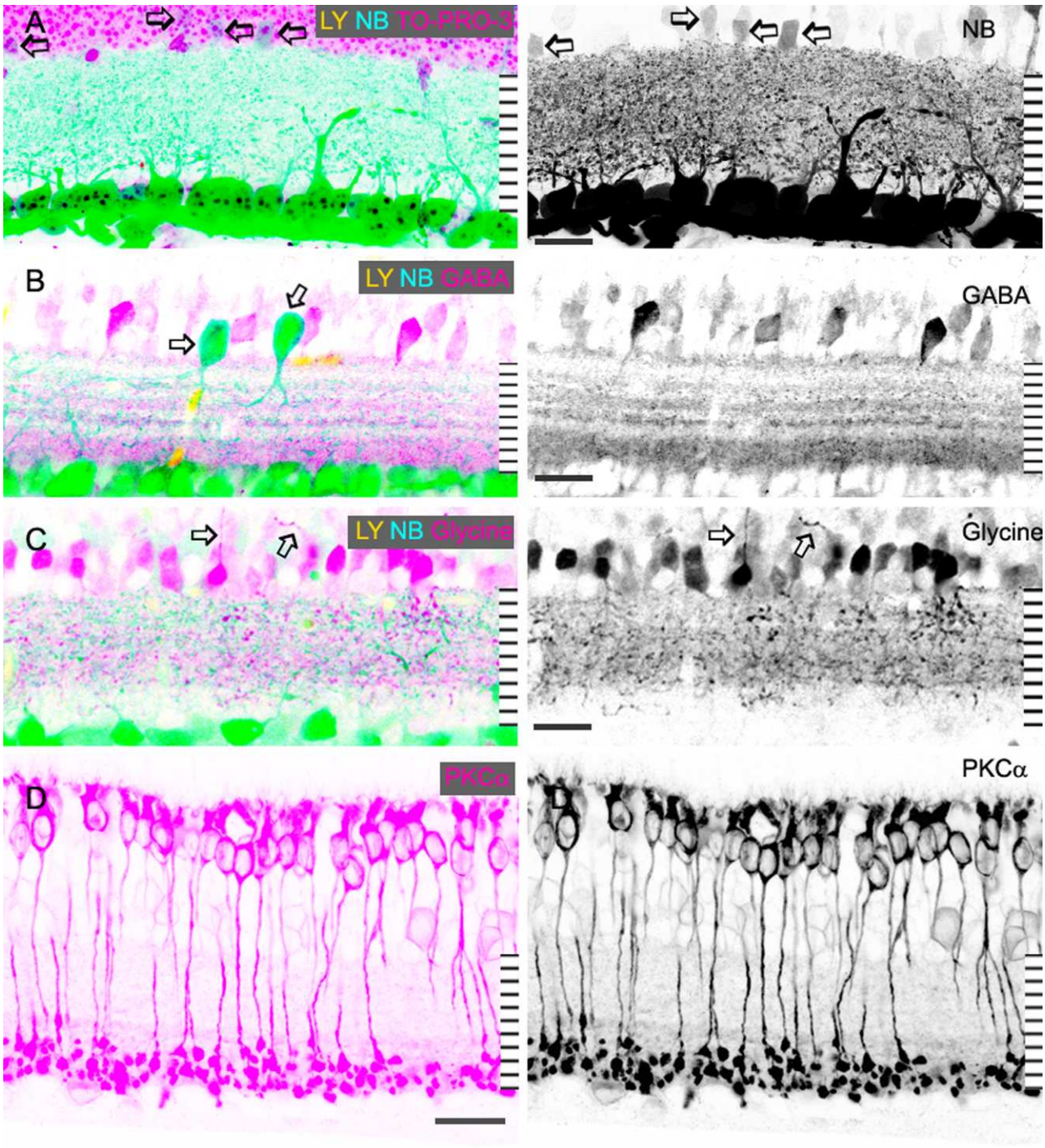

Figure 3. The composition of the IPL. Confocal micrographs of retinal vertical sections that were retrograde-labeled by LY (*yellow*) and NB (*blue*), and further stained for TO-PRO-3 (**A**), GABA (**B**), glycine (**C**) or PKCα (**D**) in *pink*. For better clarity, some color channels are showed in *black* in the *right panels*. (**A**) is a stacked and overexposed image showing the distribution of LY/NB-positive GC dendrites in the IPL. Several GC-coupled ACs negative for LY but weakly positive for NB are visible in the INL (*arrows*, [**A**]), which are clearly distinguishable from displaced GCs (*arrows*, [**B**]). GC dendrites and glycine-IR are sparse in the inner 20% of the IPL (**A**, **C**), where PKCα-positive rod bipolar cell axon terminals (**D**) and the major GABA-IR band (**B**) are located. In the distal 80% of the IPL, GC dendrites, and glycine-IR are dense. Some AC somas in the GCL and INL are weakly PKCα-IR. Axon-like processes are emitted from some strongly glycine-IR somas (*arrows*, [**C**]). *Scale bar*: 20 μm.

performed retrograde labeling in ChAT transgenic mice, whose retinal ChAT ACs were genetically labeled by td-Tomato (Fig. 6, Table). We observed that 3% of ChAT ACs in the GCL may receive NB from GCs, and these ChAT ACs were often found in the central retina. ChAT ACs in the INL were not labeled by NB in this strain of mice. These results confirm that a small number of ON-type ChAT ACs in the central retina are coupled with GCs.

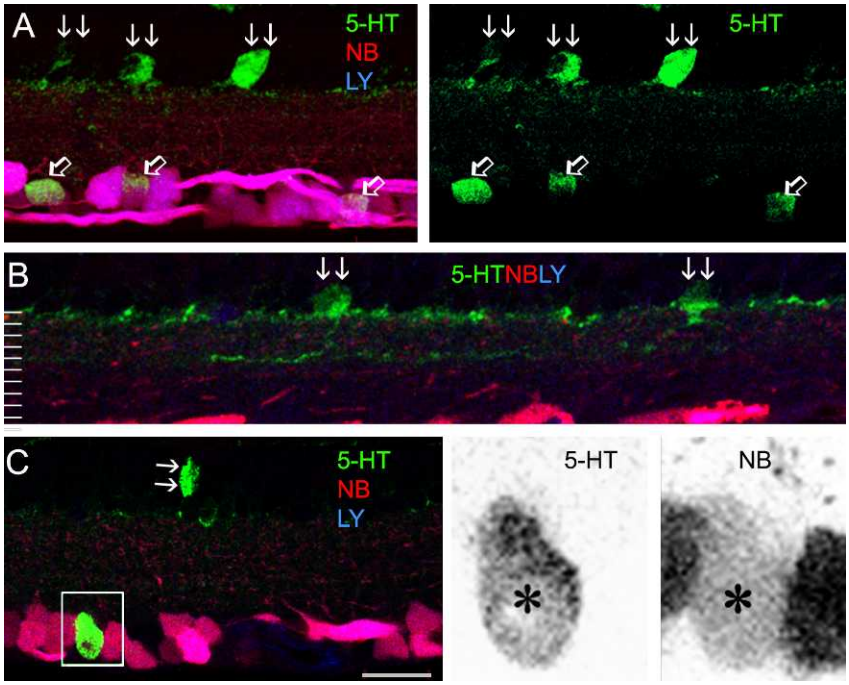

FIGURE 4. 5-HT-accumulating ACs. Confocal micrographs of retinal vertical sections that were retrograde-labeled by LY (*blue*) and NB (*red*), and further stained for 5-HT (*green*). The *green* channel in (**A**), as well as *red* and *green* channels in *insets* from (**C**), is separately presented to the *right*. 5-HT accumulating somas are located in both the GCL and INL, including GCs (positive for both LY and NB, *open arrows*, [**A**]) and ACs (LY-negative, *double arrows*, [**A**–**C**]). 5-HT-IR forms two narrow bands near 0% and 40% of the IPL depth (**B**). A GC-coupled 5-HT AC (*inset*, [**C**]) is negative for LY but positive for NB and 5-HT. *Scale bar*: 20 μm.

DISCUSSION

Overall GC-AC Coupling Is Moderate in the Mouse Retina, and it Is Dominated by Cx36 and Cx45, With the Exception of Small ACs

Although electrical coupling has been previously revealed between GCs and ACs in the mouse retina,[2,41,42] the population of GC-coupled ACs has not been reported before. Retrograde labeling is one of the most reliable ways to identify retinal GCs. By using the established double-retrograde labeling technique, we were able to label ACs that were coupled to the entire GC population and to evaluate the overall potency of the coupling between GC and AC populations. Only a fraction of all ACs was revealed to couple with GCs, demonstrating a moderate overall GC-AC coupling in the mouse retina.

Glycine and GABA have small molecular weights of 75 and 103 Da, respectively, and connexin gap junction channels are permeable to hydrophilic molecules of ~900 Da in the mammal.[63] Gap junctions between GCs and ACs likely allow GC somas to obtain the inhibitory neurotransmitter GABA,[11] and theoretically these gap junctions are permeable to glycine, as well.[9] However, GABA and glycine are widely used as AC markers[20,64] instead of GC markers. In our current and previous results, retrogradely identified GC somas were seldom positive for glycine or GABA.[11,28] Thus, GC-AC coupling did not provide GC somas with significant AC-like immunoreactivity, in keeping with the idea of moderate GC-AC coupling. In contrast to GCs, somas of cone BCs coupled to glycinergic AII ACs are clearly labeled by glycine antibody,[9,20] supporting the idea that the strength of GC-AC coupling is much weaker than that of cone BC-AII AC coupling.

The function of Cx36 and Cx45 in GC-AC coupling has been previously studied in individually labeled GCs in the mouse retina,[2,41,42] but it has not been examined in the entire GC population nor in retrogradely labeled retina before. In this study, the population of GC-coupled ACs was reduced more severely from knocking out Cx36 than from knocking out Cx45, but was not completely gone. The data was aligned with the finding from individually tracer-filled GCs[41] that Cx36 is more important than Cx45 for GC-AC coupling. Our results further indicated that some GC-AC coupling, especially in ACs with very small somas, did not depend on Cx36 or Cx45. It is unclear whether Cx30.2 mediates the coupling in these cells.[65]

In this study, the counting of total coupled ACs in the GCL was not dependent on AC markers. Although GC-coupled ACs in our results appeared to be less bright than GC somas and coupled ACs revealed by tracer-injection, their NB signals were clearly distinguishable from the background staining. The spontaneous diffusion crossing gap junctions and the large perfusion gradient of the retrograde dyes are likely responsible for the weak labeling in coupled ACs. We often optimized the exposure time so that both GCs and coupled ACs could be visualized, but GC axons and somas in our study contained high concentrations of NB, thus coupled ACs often look dimmer while GC somas are almost saturated in most micrographs. In addition, since we applied NB and LY on the cut end of the optic nerve outside the intact eyeball, dyes could potentially be taken up by GC axons, as well as astrocytes in the optic nerve. However, under our experimental conditions, LY and NB did not reveal astrocytes. Considering the continuous wrapping of Müller cells around the somas of GCs, and the completeness of the inner limiting membrane,[66,67] it is more likely that NB passing through GC-AC gap junctions, instead of NB diffusion via extracellular spaces or astrocytes, is how NB enters into the ACs.

The total number of GC-coupled ACs has not been previously reported. Intracellular NB injection in an individual GC may reveal multiple GCs and ACs,[8] which seems to predict a larger number of GC-coupled ACs than we revealed

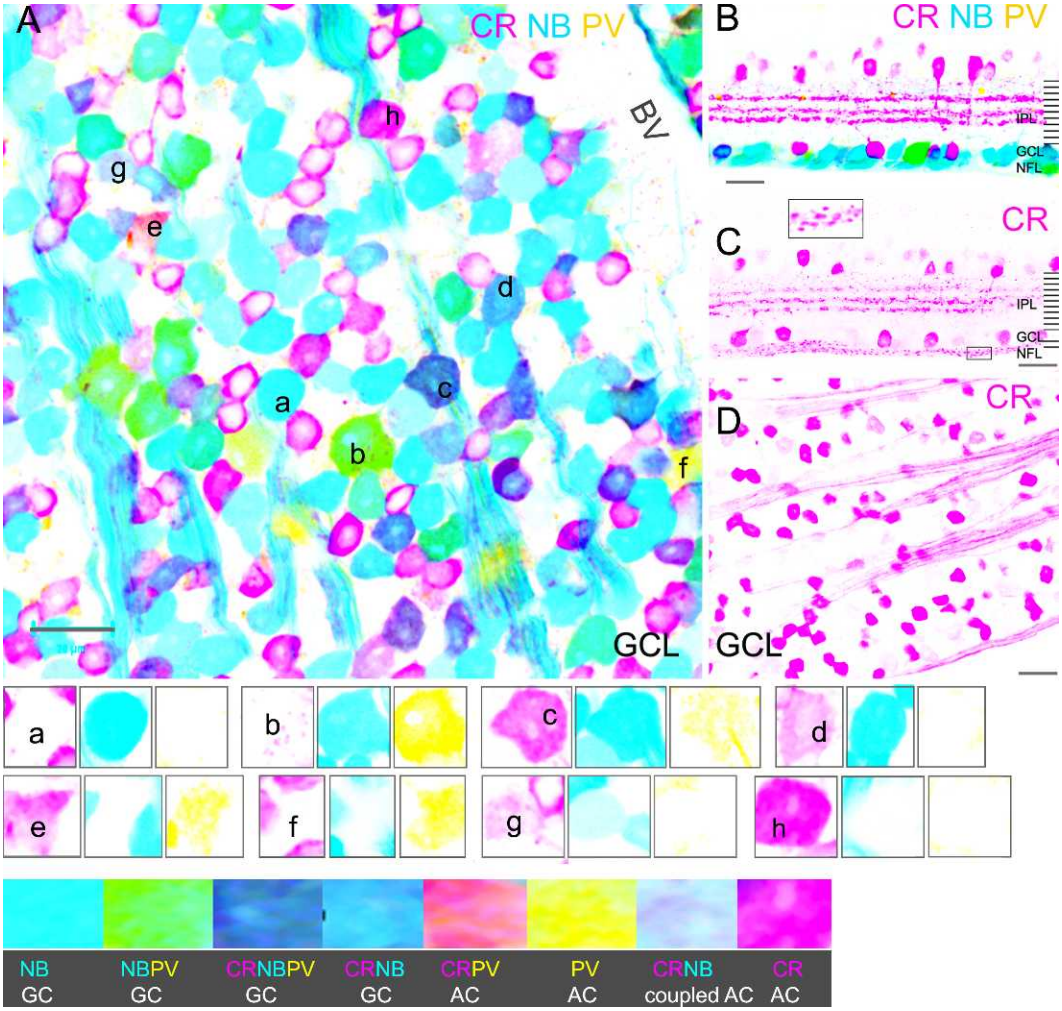

Figure 5. CR-IR and PV-IR in GCs and ACs in the mouse retina. Stacked confocal micrographs of a flat-mounted retina ([**A**], GCL) and a vertical retinal section (**B**) that were retrograde-labeled by NB (*blue*), and further stained for CR (*pink*) and PV (*yellow*). GCs and axons are brightly labeled by NB (**A**, **B**). PV-IR is colocalized in some large GC somas (*green*); and CR-IR is present in some smaller GC somas (*purple*). PV and CR also label ACs, which may contain weak to no NB signal. Confocal micrographs from a retina slice (**C**) and a flat-mounted retina ([**D**], GCL) are labeled for CR. CR-IR reveals three bright bands in the INL (**C**), somas in the INL, and GCL and axons in the NFL. Cross-sections of CR-IR axons appear to be bright small dots in the NFL (*inset*, [**C**]). The three channels of several cells in A are separately presented in the *lower panels* as small groups, with a mark in the first image of each group. (**A**–**D**) GCs. (**E**–**H**) ACs. BV, blood vessel. *Scale bar*: 20 μm.

using retrograde labeling. However, the "loyalty" of a coupled AC to the GC and the subpopulations of GCs coupled to ACs are unknown. In the mammalian retina, homologous coupling is present in certain subtypes of GCs,[8] GABA ACs,[68,69] as well as glycine ACs.[54,70] An individual GC may also be coupled with more than one subtype of AC.[8,71] In our experiments, NB was simultaneously transported into all GCs, and diffused into all ACs that directly coupled to GCs secondarily. Coupled ACs in our results showed a low NB concentration insufficient to visualize their lower-order coupling partners. Thus, even though there may be a chance that we have missed counting some coupled ACs, any missed ones are most likely those indirectly coupled with GCs. In addition, each coupled AC was only counted once in our data, no matter how many GCs or ACs it was coupled to. These reasons may explain the low percentage of ACs coupled to GCs in our data, and in conjunction with previous findings,[8,71] further suggest coupling between one AC and multiple GCs.

GC-AC Coupling Is Mostly Located in the Distal 80% of the IPL and Favors GABA ACs More Than Glycine ACs

In a few subtypes of GCs, chemical inputs from GABA ACs seem to be critical,[40,72–75] but the differential contribution of GABA ACs and glycine ACs to the overall GC-AC coupling is largely unknown.[8,12,13] Our results reveal that in the GCL, GABA ACs are about six times more prevalent than glycine ACs among the GC-coupled ACs. However, the populations of these two subtypes of GC-coupled ACs are nearly equal in the INL, considering GABA ACs and glycine ACs each comprise nearly half of the total AC population.[21,58–62] This data indicates that the coupling between GABAergic ACs and GCs is more intensive and likely more important than that between glycinergic ACs and GCs. Our data is in line with the fact that GABA ACs are the most frequently reported ACs coupled with GCs.[39,40] The result may be explained by the relatively large stratified dendritic arbors of most GABA ACs and GCs but small

Investigative Ophthalmology & Visual Science

Table. Fraction of Some Tracer-Coupled ACs

Soma Location	AC	Cells, *n*	NB-Positive AC	
			Cells, *n*	%
GCL	ChAT-IR	401	8	2.0
	ChAT-tdTomato	251	8	3.2
	5-HT-IR	160	15	9.4
INL	GABA-IR	383	16	4.2
	Glycine-IR	176	7	4.0
	ChAT-IR	212	0	0.0
	ChAT-tdTomato	349	0	0.0
	bNOS-IR	60	4	6.7
	5-HT-IR	59	6	10.2

Number of AC-IRs for an AC marker and negative for LY, as well as the number of LY-negative/NB-positive ones in that group.

and diffuse dendritic trees of glycine ACs,[6,14,15] given that GCs make gap-junctional contacts with ACs at their dendrites.[2]

More than 20 morphological subtypes of GCs have been reported so far,[8,12,13] and 15 subtypes were reported to couple with ACs.[8] However, populations of the coupled GCs have not been previously reported, thus the density and distribution of GC-AC coupling sites in the IPL have not been evaluated previously. Conventional GCs send dendrites mostly to 20% to 80% of the IPL depth.[8,12,13] Displaced GCs send dendrites to 0% to 80% of the IPL depth, except for dG2 cells, whose dendritic arbor covers 75% to 100% of the IPL depth.[11] Our current data showed that dendrites of retrogradely identified GCs were nearly evenly distributed in the distal 80% of the IPL but were sparse in the inner 20%. This data, in agreement with previous findings, indicates that a great majority of GCs ramify in the distal 80% of the IPL. Furthermore, using GC somas and AC somas as IPL boundaries, we observed that the colocalization of NB with GABA-IR or glycine-IR was primarily located in the distal 80% of the IPL. These data together suggest that GC-AC coupling sites are mainly distributed in the distal 80% of the IPL and involve both conventional and displaced GCs.

GABA ACs are usually stratified in the IPL, while glycine ACs are diffusely ramifying.[6,20,21,48] It has been unknown whether glycine and GABA inputs vary among any strata in the IPL. A heavy GABA-IR band is present in the inner 20% of IPL,[20] but out of eight total subtypes of glycinergic ACs, only two subtypes (AII and type4) send dendrites to the inner 20% of the IPL in the murine retina.[21] In line with these reports, our results show that the inner 20% of the IPL contains rich GABA-IR, sparse glycine-IR, and rod bipolar cell terminals. The results suggest that GABA ACs are the dominant ACs in the inner 20% of the IPL, especially for rod bipolar cells and those ON GCs that send processes exclusively to that stratum.

Several Immunological Subtypes of ACs Can Couple to GCs, But Not All of the ACs in the Same Subpopulation Participate in the Coupling

In the mouse retina, only some GABA ACs[39,40] and some NI ACs[28] have been reported to couple to GCs. 5-HT-accumulating ACs have not been reported previously in the mouse retina, and the labeling of PV and CR has not been examined in retrogradely labeled retinas before. GC-coupled ACs are located in both the GCL and INL.[8,9] Our results, in line with these findings, further reveal that a variety of ACs could couple to GCs, which include GABA-IR, glycine-IR, NI ACs, ChAT ACs, 5-HT-accumulating, and CR-IR ACs. GC-AC coupling occurred only in a small portion of these subtypes of ACs, demonstrating that the immunoreactivity of ACs is not a definite indicator for their coupling pattern with GCs.

Individual tracer-filled starburst ACs and direction-selective GCs[76,77] have not been reported to be coupled with each other. These previous studies partially support our results that ChAT ACs in the INL are not coupled with GCs. But in the GCL, our data showed that a small number of brightly ChAT-IR ACs and tdTomato-labeled ChAT ACs were NB-positive. These ChAT cells were often located in the central retina. The different coupling rate for displaced and conventional ChAT ACs seems to be function-related, as ChAT ACs in the GCL are ON-center cells, while ChAT ACs in the INL are OFF-center cells.[6,78] Somas of ChAT ACs in the GCL may form small clusters, and they are distributed less uniformly than those in the INL (Figs. 2, 6).[22,79] Our result can be compared with the published data obtained from individually dye-injected GCs, in which some GC-coupled ACs possessed mono-stratified dendritic arbors at the location of the ON-ChAT band (i.e., the ACs coupled to $G_{1,2,6}$).[8] ChAT ACs are one of the only known types of ACs in the mammalian retina that have mono-stratified dendritic trees at that stratum.[6,14,15] Since we investigated GCs in whole retinas (around 50,000 GCs per retina),[11,80] less frequent GC-AC coupling is more likely to be revealed in our experiments. However, developmental defects may not be completely ruled out, as an explanation for the coupled ChAT cells.

In other studies, PV has been used to label GCs in the mouse retina[29] and AII ACs in the rabbit[30] and rat retina.[31] CR was reported to label most GCs[32] in the mouse retina, but stain

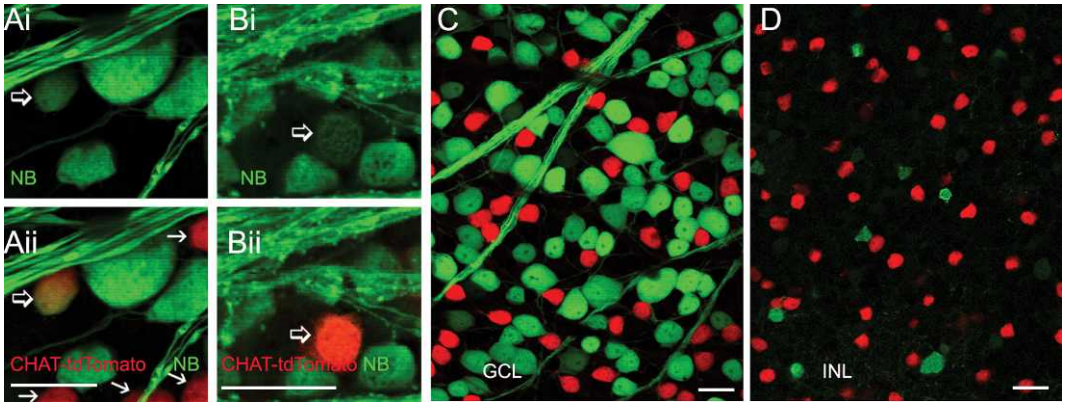

Figure 6. NB-labeled ChAT ACs in ChAT transgenic mice. The flat-mount retinas were retrograde-labeled by NB (*green*), and ChAT ACs are genetically labeled by tdTomato (*red*, [**A**–**D**]; *arrows*, [**A**, **B**]). Some brightly labeled ChAT ACs are weakly NB-positive ([**A**, **B**], *open arrows*), indicating that they are coupled to GCs. *Scale bar*: 20 μm.

Investigative Ophthalmology & Visual Science

multiple types of retinal neurons in other species.[33,34] With GCs being retrogradely identified, our results demonstrate that neither GCs nor ACs can be safely identified by PV-IR or CR-IR in the mouse retina. Some CR-IR ACs were found to couple to GCs. Considering the large population size, CR-IR ACs may not be a homogeneous population of ACs. Further studies are required to identify the subtypes that were coupled to GCs.

Depolarizing Electrical Outputs From Coupled ACs

Outputs of ACs at chemical synapses have opposite polarity from their electrical synapses, because depolarization of the cells increases their inhibitory neurotransmitter release. Polarities of outputs from ACs coupled to GCs are dependent on membrane potentials and reversal potentials of light responses, as well. In the vertebrate retina, ACs mostly generate depolarizing ON and depolarizing ON-OFF light responses, and the reversal potentials of light responses often fall between 0 to approximately −30 mV.[3,7] It is about 0 to approximately −10 mV for NI ACs in the mouse retina,[28] with the chloride equilibrium potential being set to approximately −60 mV. For these cells, light-evoked membrane currents are usually outward (hyperpolarizing) when the holding potential is above the reversal potential and inward (depolarizing) when the holding potential is below the reversal potential. Only a minority of ACs are hyperpolarized during light on, (e.g., glycinergic ACs gly1, gly2, and gly6).[7] Such sustained hyperpolarizing light responses usually do not have clear reversal potentials. Thus, it is likely that most GC-coupled ACs could provide depolarizing electrical outputs at a membrane potential below the reversal potential, as expected in most physiological conditions, though the overall impedance load may not be so significant.

In the mammalian brain, electrical coupling is a fundamental feature of local inhibitory circuits, and electrical synapses define functionally diverse networks of GABA-releasing interneurons.[81,82] In the mammalian retina, the heterologous coupling between GCs and GABA ACs was found to be responsible for the short-latency concerted synchronous spiking activity of neighboring OFF-α-GCs.[83] The significance of the coupling between diverse subtypes of ACs and GCs is still largely unknown.

Acknowledgments

We thank Roy Jacoby, Ruth Ritter, and Scott Young for editing this manuscript.

Supported by National Institutes of Health (NIH) Grant 1F32 EY13915 and Knights Templar Eye Foundation (J-JP) and by NIH Grant EY 004446; EY 019908; NIH Vision Core Grant EY 02520; the Retina Research Foundation (Houston, Texas); and Research to Prevent Blindness, Inc. (SMW).

Disclosure: **J-J. Pang**, None; **D.L. Paul**, None; **S.M. Wu**, None

References

1. Vaney DI. Many diverse types of retinal neurons show tracer coupling when injected with biocytin or Neurobiotin. *Neurosci Lett*. 1991;125:187–190.
2. Schubert T, Degen J, Willecke K, Hormuzdi SG, Monyer H, Weiler R. Connexin36 mediates gap junctional coupling of alpha-ganglion cells in mouse retina. *J Comp Neurol*. 2005; 485:191–201.
3. Pang JJ, Gao F, Wu SM. Segregation and integration of visual channels: layer-by-layer computation of ON-OFF signals by amacrine cell dendrites. *J Neurosci*. 2002;22:4693–4701.
4. Dacheux RF, Raviola E. The rod pathway in the rabbit retina: a depolarizing bipolar and amacrine cell. *J Neurosci*. 1986;6: 331–345.
5. Dacheux RF, Raviola E. Light responses from one type of ON-OFF amacrine cells in the rabbit retina. *J Neurophysiol*. 1995; 74:2460–2468.
6. Kolb H. Amacrine cells of the mammalian retina: neurocircuitry and functional roles. *Eye (Lond)*. 1997;11:904–923.
7. Pang JJ, Gao F, Wu SM. Physiological characterization and functional heterogeneity of narrow-field mammalian amacrine cells. *J Physiol*. 2012;590:223–234.
8. Volgyi B, Chheda S, Bloomfield SA. Tracer coupling patterns of the ganglion cell subtypes in the mouse retina. *J Comp Neurol*. 2009;512:664–687.
9. Vaney DI, Nelson JC, Pow DV. Neurotransmitter coupling through gap junctions in the retina. *J Neurosci*. 1998;18: 10594–10602.
10. Mills SL, Massey SC. Differential properties of two gap junctional pathways made by AII amacrine cells. *Nature*. 1995;377:734–737.
11. Pang JJ, Wu SM. Morphology and immunoreactivity of retrogradely double-labeled ganglion cells in the mouse retina. *Invest Ophthalmol Vis Sci*. 2011;52:4886–4896.
12. Badea TC, Nathans J. Quantitative analysis of neuronal morphologies in the mouse retina visualized by using a genetically directed reporter. *J Comp Neurol*. 2004;480:331–351.
13. Sun W, Li N, He S. Large-scale morphological survey of mouse retinal ganglion cells. *J Comp Neurol*. 2002;451:115–126.
14. MacNeil MA, Heussy JK, Dacheux RF, Raviola E, Masland RH. The shapes and numbers of amacrine cells: matching of photofilled with Golgi-stained cells in the rabbit retina and comparison with other mammalian species. *J Comp Neurol*. 1999;413:305–326.
15. Kolb H, Linberg KA, Fisher SK. Neurons of the human retina: a Golgi study. *J Comp Neurol*. 1992;318:147–187.
16. Mitrofanis J, Provis JM. A distinctive soma size gradient among catecholaminergic neurones of human retinae. *Brain Res*. 1990;527:69–75.
17. Dacey DM. Axon-bearing amacrine cells of the macaque monkey retina. *J Comp Neurol*. 1989;284:275–293.
18. Taylor WR. Response properties of long-range axon-bearing amacrine cells in the dark-adapted rabbit retina. *Vis Neurosci*. 1996;13:599–604.
19. Masland RH. The fundamental plan of the retina. *Nat Neurosci*. 2001;4:877–886.
20. Haverkamp S, Wassle H. Immunocytochemical analysis of the mouse retina. *J Comp Neurol*. 2000;424:1–23.
21. Menger N, Pow DV, Wassle H. Glycinergic amacrine cells of the rat retina. *J Comp Neurol*. 1998;401:34–46.
22. Zhang J, Yang Z, Wu SM. Development of cholinergic amacrine cells is visual activity-dependent in the postnatal mouse retina. *J Comp Neurol*. 2005;484:331–343.
23. Witkovsky P. Dopamine and retinal function. *Doc Ophthalmol*. 2004;108:17–40.
24. Nguyen-Legros J, Versaux-Botteri C, Savy C. Dopaminergic and GABAergic retinal cell populations in mammals. *Microsc Res Tech*. 1997;36:26–42.
25. Djamgoz MB, Wagner HJ. Localization and function of dopamine in the adult vertebrate retina. *Neurochem Int*. 1992;20:139–191.
26. Haverkamp S, Kolb H, Cuenca N. Morphological and neurochemical diversity of neuronal nitric oxide synthase-positive amacrine cells in the turtle retina. *Cell Tissue Res*. 2000;302:11–19.

27. Oh SJ, Kim IB, Lee MY, Chun MH, Chung JW. NOS-like immunoreactive neurons express GABA-like immunoreactivity in rabbit and rat retinae. *Exp Brain Res*. 1998;120:109–113.
28. Pang JJ, Gao F, Wu SM. Light responses and morphology of bNOS-immunoreactive neurons in the mouse retina. *J Comp Neurol*. 2010;518:2456–2474.
29. Kim TJ, Jeon CJ. Morphological classification of parvalbumin-containing retinal ganglion cells in mouse: single-cell injection after immunocytochemistry. *Invest Ophthalmol Vis Sci*. 2006; 47:2757–2764.
30. Casini G, Rickman DW, Brecha NC. AII amacrine cell population in the rabbit retina: identification by parvalbumin immunoreactivity. *J Comp Neurol*. 1995;356:132–142.
31. Wassle H, Grunert U, Rohrenbeck J. Immunocytochemical staining of AII-amacrine cells in the rat retina with antibodies against parvalbumin. *J Comp Neurol*. 1993;332:407–420.
32. Lee ES, Lee JY, Jeon CJ. Types and density of calretinin-containing retinal ganglion cells in mouse. *Neurosci Res*. 2010; 66:141–150.
33. Hwang IK, Yoo KY, Kim DS, et al. Comparative study on calretinin immunoreactivity in gerbil and rat retina. *Anat Histol Embryol*. 2005;34:129–131.
34. Grana P, Anadon R, Yanez J. Immunocytochemical study of calretinin and calbindin D-28K expression in the retina of three cartilaginous fishes and a cladistian (Polypterus). *Brain Res Bull*. 2008;75:375–378.
35. Richmond FJ, Gladdy R, Creasy JL, Kitamura S, Smits E, Thomson DB. Efficacy of seven retrograde tracers, compared in multiple-labelling studies of feline motoneurones. *J Neurosci Methods*. 1994;53:35–46.
36. Kobbert C, Apps R, Bechmann I, Lanciego JL, Mey J, Thanos S. Current concepts in neuroanatomical tracing. *Prog Neurobiol*. 2000;62:327–351.
37. Drager UC, Olsen JF. Ganglion cell distribution in the retina of the mouse. *Invest Ophthalmol Vis Sci*. 1981;20:285–293.
38. Keyser KT, Britto LR, Woo JI, Park DH, Joh TH, Karten HJ. Presumptive catecholaminergic ganglion cells in the pigeon retina. *Vis Neurosci*. 1990;4:225–235.
39. Muller LP, Do MT, Yau KW, He S, Baldridge WH. Tracer coupling of intrinsically photosensitive retinal ganglion cells to amacrine cells in the mouse retina. *J Comp Neurol*. 2010;518: 4813–4824.
40. Sivyer B, Vaney DI. Dendritic morphology and tracer-coupling pattern of physiologically identified transient uniformity detector ganglion cells in rabbit retina. *Vis Neurosci*. 2010; 27:159–170.
41. Pan F, Paul DL, Bloomfield SA, Volgyi B. Connexin36 is required for gap junctional coupling of most ganglion cell subtypes in the mouse retina. *J Comp Neurol*. 2010;518:911–927.
42. Schubert T, Maxeiner S, Kruger O, Willecke K, Weiler R. Connexin45 mediates gap junctional coupling of bistratified ganglion cells in the mouse retina. *J Comp Neurol*. 2005;490: 29–39.
43. Pang JJ, Gao F, Wu SM. Light-evoked excitatory and inhibitory synaptic inputs to ON and OFF alpha ganglion cells in the mouse retina. *J Neurosci*. 2003;23:6063–6073.
44. Ghosh KK, Bujan S, Haverkamp S, Feigenspan A, Wassle H. Types of bipolar cells in the mouse retina. *J Comp Neurol*. 2004;469:70–82.
45. Cook JE, Becker DL. Gap junctions in the vertebrate retina. *Microsc Res Tech*. 1995;31:408–419.
46. Deans MR, Volgyi B, Goodenough DA, Bloomfield SA, Paul DL. Connexin36 is essential for transmission of rod-mediated visual signals in the mammalian retina. *Neuron*. 2002;36: 703–712.
47. Blankenship AG, Hamby AM, Firl A, et al. The role of neuronal connexins 36 and 45 in shaping spontaneous firing patterns in the developing retina. *J Neurosci*. 2011;31:9998–10008.
48. Zhang J, Yang Z, Wu SM. Immuocytochemical analysis of spatial organization of photoreceptors and amacrine and ganglion cells in the tiger salamander retina. *Vis Neurosci*. 2004;21:157–166.
49. Pow DV, Wright LL, Vaney DI. The immunocytochemical detection of amino-acid neurotransmitters in paraformaldehyde-fixed tissues. *J Neurosci Methods*. 1995;56:115–123.
50. Haverkamp S, Ghosh KK, Hirano AA, Wassle H. Immunocytochemical description of five bipolar cell types of the mouse retina. *J Comp Neurol*. 2003;455:463–476.
51. Elshatory Y, Everhart D, Deng M, Xie X, Barlow RB, Gan L. Islet-1 controls the differentiation of retinal bipolar and cholinergic amacrine cells. *J Neurosci*. 2007;27:12707–12720.
52. Huang PL, Lo EH. Genetic analysis of NOS isoforms using nNOS and eNOS knockout animals. *Prog Brain Res*. 1998;118: 13–25.
53. Mills SL, Massey SC. Differential properties of two gap junctional pathways made by AII amacrine cells. *Nature*. 1995;377:734–737.
54. Bloomfield SA, Xin D, Osborne T. Light-induced modulation of coupling between AII amacrine cells in the rabbit retina. *Vis Neurosci*. 1997;14:565–576.
55. Mills SL, Xia XB, Hoshi H, et al. Dopaminergic modulation of tracer coupling in a ganglion-amacrine cell network. *Vis Neurosci*. 2007;24:593–608.
56. Ribelayga C, Mangel SC. Tracer coupling between fish rod horizontal cells: modulation by light and dopamine but not the retinal circadian clock. *Vis Neurosci*. 2007;24:333–344.
57. Mrini A, Moukhles H, Jacomy H, Bosler O, Doucet G. Efficient immunodetection of various protein antigens in glutaraldehyde-fixed brain tissue. *J Histochem Cytochem*. 1995;43: 1285–1291.
58. Yazulla S, Yang CY. Colocalization of GABA and glycine immunoreactivities in a subset of retinal neurons in tiger salamander. *Neurosci Lett*. 1988;95:37–41.
59. Zhang J, Yang Z, Wu SM. Immuocytochemical analysis of spatial organization of photoreceptors and amacrine and ganglion cells in the tiger salamander retina. *Vis Neurosci*. 2004;21:157–166.
60. Yang CY, Yazulla S. Light microscopic localization of putative glycinergic neurons in the larval tiger salamander retina by immunocytochemical and autoradiographical methods. *J Comp Neurol*. 1988;272:343–357.
61. Yang CY, Yazulla S. Localization of putative GABAergic neurons in the larval tiger salamander retina by immunocytochemical and autoradiographic methods. *J Comp Neurol*. 1988;277:96–108.
62. Crook DK, Pow DV. Analysis of the distribution of glycine and GABA in amacrine cells of the developing rabbit retina: a comparison with the ontogeny of a functional GABA transport system in retinal neurons. *Vis Neurosci*. 1997;14:751–763.
63. Veenstra RD. Size and selectivity of gap junction channels formed from different connexins. *J Bioenerg Biomembr*. 1996;28:327–337.
64. Strettoi E, Masland RH. The number of unidentified amacrine cells in the mammalian retina. *Proc Natl Acad Sci U S A*. 1996; 93:14906–14911.
65. Muller LP, Dedek K, Janssen-Bienhold U, et al. Expression and modulation of connexin 30.2, a novel gap junction protein in the mouse retina. *Vis Neurosci*. 2010;27:91–101.
66. Holländer H, Makarov F, Dreher Z, van Driel D, Chan-Ling TL, Stone J. Structure of the macroglia of the retina: sharing and

Investigative Ophthalmology & Visual Science

division of labour between astrocytes and Muller cells. *J Comp Neurol*. 1991;313:587–603.

67. Ramirez JM, Trivino A, Ramirez AI, Salazar JJ, Garcia-Sanchez J. Structural specializations of human retinal glial cells. *Vision Res*. 1996;36:2029–2036.
68. Vaney DI. Type 1 nitrergic (ND1) cells of the rabbit retina: comparison with other axon-bearing amacrine cells. *J Comp Neurol*. 2004;474:149–171.
69. Wright LL, Vaney DI. The type 1 polyaxonal amacrine cells of the rabbit retina: a tracer-coupling study. *Vis Neurosci*. 2004; 21:145–155.
70. Wright LL, Macqueen CL, Elston GN, Young HM, Pow DV, Vaney DI. The DAPI-3 amacrine cells of the rabbit retina. *Vis Neurosci*. 1997;14:473–492.
71. Jacoby R, Stafford D, Kouyama N, Marshak D. Synaptic inputs to ON parasol ganglion cells in the primate retina. *J Neurosci*. 1996;16:8041–8056.
72. Vaney DI, Sivyer B, Taylor WR. Direction selectivity in the retina: symmetry and asymmetry in structure and function. *Nat Rev Neurosci*. 2012;13:194–208.
73. Taylor WR, Smith RG. The role of starburst amacrine cells in visual signal processing. *Vis Neurosci*. 2012;29:73–81.
74. Briggman KL, Helmstaedter M, Denk W. Wiring specificity in the direction-selectivity circuit of the retina. *Nature*. 2011; 471:183–188.
75. Lee S, Kim K, Zhou ZJ. Role of ACh-GABA cotransmission in detecting image motion and motion direction. *Neuron*. 2010; 68:1159–1172.
76. Vardi N, Masarachia PJ, Sterling P. Structure of the starburst amacrine network in the cat retina and its association with alpha ganglion cells. *J Comp Neurol*. 1989;288:601–611.
77. Chen YC, Chiao CC. Symmetric synaptic patterns between starburst amacrine cells and direction selective ganglion cells in the rabbit retina. *J Comp Neurol*. 2008;508:175–183.
78. Lee S, Zhou ZJ. The synaptic mechanism of direction selectivity in distal processes of starburst amacrine cells. *Neuron*. 2006;51:787–799.
79. Rodieck RW, Marshak DW. Spatial density and distribution of choline acetyltransferase immunoreactive cells in human, macaque, and baboon retinas. *J Comp Neurol*. 1992;321:46–64.
80. Jeon CJ, Strettoi E, Masland RH. The major cell populations of the mouse retina. *J Neurosci*. 1998;18:8936–8946.
81. Galarreta M, Hestrin S. Spike transmission and synchrony detection in networks of GABAergic interneurons. *Science*. 2001;292:2295–2299.
82. Galarreta M, Hestrin S. Electrical synapses between GABA-releasing interneurons. *Nat Rev Neurosci*. 2001;2:425–433.
83. Hu EH, Bloomfield SA. Gap junctional coupling underlies the short-latency spike synchrony of retinal alpha ganglion cells. *J Neurosci*. 2003;23:6768–6777.

Investigative Ophthalmology & Visual Science